Mine Water and the Environment (2024) 43:382–398
https://doi.org/10.1007/s10230-024-00981-7

TECHNICAL ARTICLE

A Novel Method for In-Situ Monitoring and Quantifying the Dynamic Responses of Groundwater to the Effects of Mining

Shihao Meng[1,2,3] · Qiang Wu[1,2,3] · Yifan Zeng[1,2,3] · Chao Yu[1] · Xiaoxiu Liu[1] · Lu Wang[4] · Lei Yang[5] · Yao Zhang[1]

Received: 21 November 2023 / Accepted: 26 April 2024 / Published online: 15 June 2024
© The Author(s) under exclusive licence to International Mine Water Association 2024

Abstract

Accurately exploring whether fractures are interconnected and whether water can flow through them, as well as quantitatively describing how underground water systems are affected by mining activities, is crucial for the safe exploitation of mineral resources and for protecting ecological water resources. Traditional groundwater level monitoring and geophysical techniques are unable to visualize many of these mining-triggered effects on the hydrological system, as well as the sources and vertical seepage paths of water inflow. A method combining particle-magnetic heading optical tracking technology (PMHOTT) and an artificial tracer test was proposed to address this problem. This method tracks and calibrates the water flow rate, velocity, direction, and dynamic composition of water flowing into the working face through in-situ monitoring and multi-aquifer tracer penetration flux-time relationship analysis. By analyzing hydrological metrics, the impact of mining activities on the groundwater system and the dynamic changes of the flow field within the effective influence area can be determined. The results indicate that the PMHOTT monitoring data, after correction, overcame the deficiency of insufficient observation boreholes in traditional water level monitoring, and accurately captured flow field changes in the area most affected by mining activities. Meanwhile, by considering the interaction between multiple tracers, we successfully identified the sources of water inflow entering the mine as well as the groundwater seepage path. This study accurately evaluated the development height of water-conducting fractures and quantified groundwater flow time, expanding the applicability of artificial tracer test in the fractured aquifer. This will be useful for predicting and preventing mining water hazards under complex hydrogeological conditions.

Keywords Tracer test · Mining water hazards · Water-conducting fracture · Flow velocity · fracture flow

Introduction

Mining-related activities can generate and expand fractures, which can alter the permeability of rock formations and reduce their water barrier properties. In such cases, water resources may be lost or water-related accidents may occur (Cheng et al. 2020). In addition, the deformation of overlying strata can lead to changes in porosity and permeability parameters. Changes in dynamic and static water pressure and permeability also affect the stress and strain of overlying strata. This interaction also enlarges fractures and fissures and promotes groundwater movement. Therefore, it is important for the safe development of mining resources and protection of ecological water resources to quantitatively characterize the nonlinear and time-varying hydrogeological system of mining-induced deformation of overlying strata, and to study the dynamic changes of groundwater systems in time and space during the mining process.

✉ Yifan Zeng
zengyf@cumtb.edu.cn

1 National Engineering Research Center for Controlling Coal Mine Water Hazards Controlling, China University of Mining and Technology, Beijing 100083, China

2 National Mine Safety Administration Key Laboratory for Controlling Coal Mine Water Hazards, Beijing 100083, China

3 University of Mining and Technology (Beijing) Inner Mongolia Research Institute, Ordos 017000, Inner Mongolia, China

4 Shaanxi Coal Caojiatan Mining Co., Ltd., Shaanxi 719000, China

5 Shenmu Hongliulin Mining Co Ltd of Shaanxi Coal Group, Shaanxi 719300, China

The effects of mining on the groundwater system can be divided into three stages: advance drainage, local damage, and regional driving. In the advance drainage stage, water must be released from the overlying aquifer in advance to ensure production safety. Local damage occurs during mining when the overlying rock structure is disrupted, potentially forming major drainage channels in the groundwater system. During the post-mining regional driving stage, the formation of water-conducting fracture zones can cause changes in the recharge, discharge, and runoff of the entire groundwater system. In-situ detection and monitoring are direct methods that can be used to predict and explore the development characteristics of water-conducting fracture zones.

The more commonly used detection and monitoring methods can be broadly categorized into two types. The first type includes drilling techniques, such as borehole three-dimensional imaging (Zhu et al. 2010) and borehole flushing fluid methods (State Bureau of Coal Industry 2000). The second type involves geophysical techniques, such as electrical (Yeh et al. 2015), electromagnetic (Qamar et al. 2019), and microseismic methods (Lai et al. 2021). However, these methods are mainly used to detect fractures in rocks and have two major disadvantages: it is impossible to accurately determine whether the detected cracks are water-conducting or if the detected fractures are connected to the underground mines. Therefore, besides investigating the fractures caused by overlying rock damage, it is essential to study the dynamic changes of the groundwater system to ensure the safe exploitation of mining resources.

Identifying the path and time of groundwater flowing into the mine through mining-induced fractures is highly challenging. Groundwater tracer technology is often used to study the flow and contamination flow pathways of groundwater (Wang et al. 2022). It involves introducing artificial tracers, such as chemicals with specific properties or radioactive isotopes, into the groundwater system to track the flow and mixing of groundwater. This technology is widely applied in water resources management (Pinasseau et al. 2023), groundwater pollution research (He et al. 2022), groundwater recharge (Burnett et al. 2010), and watershed hydrology (Laurent et al. 2015). It helps us understand the characteristics of groundwater flow, assess the sustainability of water resources, and provide a scientific basis for groundwater protection and management. In underground rivers and karst groundwater systems, artificial tracer tests are particularly effective and have advantages in terms of time and space (Qi et al. 2018). Through this technology, the flow path of groundwater in complex underground karst channels can be tracked, providing a deeper understanding of the relationship between groundwater and underground dissolution processes. However, inferring the process of groundwater movement caused by mining with traditional detection methods is not sufficiently intuitive (Zeng et al. 2024). On the other hand, tracer tests in fractured aquifers face limitations and challenges due to heterogeneity. The difficulty of this lies in applying tracer techniques that can intuitively reflect groundwater movement to these fractured aquifers.

The Ordos Coalfield is the largest coalfield in China and holds an important position in the China's Western Development Strategy (Ning 2013). With the widespread adoption of comprehensive mechanized mining and large-scale high-extraction thickness mining methods, the characteristics of massive strata deformation and nonlinear evolution of the groundwater system will become more prominent. This study was undertaken to analyze the horizontal seepage characteristics of groundwater based on particle-magnetic heading optical tracking technology (PMHOTT) groundwater level (GWL) measurements, flow velocities, and directions in hydrological monitoring wells. Building on this, artificial tracer tests will be conducted by introducing different tracers and real-time monitoring in the mine to determine the vertical seepage characteristics of groundwater. By quantifying the transit time of groundwater and determining the flow paths, the applicability of artificial tracer tests in fractured aquifers can be expanded, providing assistance in predicting and preventing mine water hazards under complex hydrogeological conditions.

Study Area

The Caojiatan Coalfield is located in the northeastern part of the Ordos Plateau, north of the Loess Plateau in northern Shaanxi Province, and on the southeastern edge of the Maowusu Desert (Fig. 1a). It is characterized by sand dunes, sandy and wind-blown land, and loess landforms. The coalfield covers an area of 108.49 km^2 and has five main coal seams with a total estimated recoverable reserves of 1.51×10^8 t. The current main extraction is conducted at a depth of ≈ 300 m in the 2–2 coal seam, with an annual output of about 1.70×10^7 t. In the central part of the mining area, there is a NW to SE oriented watershed that divides the groundwater into two relatively independent hydrogeological units: the southwest belongs to the Yuxi River basin and the northeast belongs to the Tuwei River basin (Fig. 1b). The mining area has abundant coal resources, limited water resources, a simple geological structure, and a fragile ecology.

Hydrogeological Characteristics

Based on the occurrence conditions and hydraulic characteristics of the groundwater, the aquifers above the main coal seam can be generalized into four categories. The uppermost is the Quaternary aquifer, which includes the Quaternary

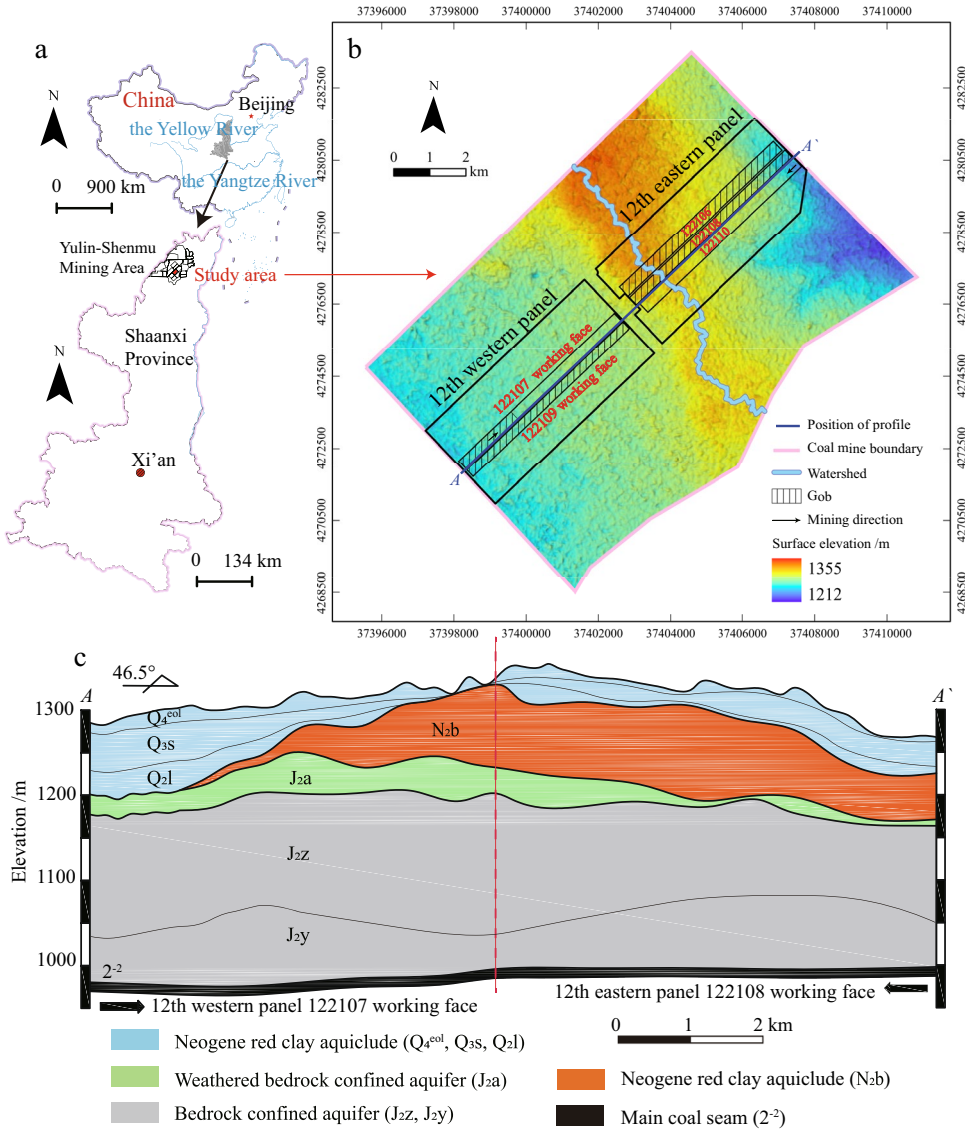

Fig. 1 The geographical location and hydrogeologic profile of the coal mine

Aeolian deposits (Q_4^{eol}), the Upper Pleistocene Salawusu Formation (Q_3s), and the Middle Pleistocene Lishi Formation (Q_2l). The Salawusu Formation mainly consists of fine sand with occasional medium to coarse sand. It is highly receptive to recharge from atmospheric precipitation and has a moderate level of water abundance. Below the aquifer lies a key aquitard composed of red clay from the Neogene Baode Formation (N_2b). Its ability to prevent water flow is directly related to mine safety and serves as an important guarantee for water security in industry, agriculture, domestic use, and ecology. Beneath the unconsolidated formation, there is the fractured aquifer of the Middle Jurassic strata, including the Middle Jurassic Anding Formation (J_2a), Zhiluo Formation (J_2z), and Yan'an Formation (J_2y). These formations consist primarily of medium to fine sandstone. Additionally, due to the influence of paleotopography, the top surface of the rocks underwent varying degrees of weathering. The entire Anding Formation in the region is a weathered bedrock section with an average thickness of 20 m. Therefore, the bedrock section is divided into a weathered bedrock aquifer and a bedrock aquifer. The weathered bedrock has a jumbled structure, is soft and fragile, and has enlarged pore spaces, resulting in increased permeability. The normal bedrock has a compact structure and less water abundance.

Factors Contributing to Mine Inflow

(1) Water-conducting channel (s): there is no water-conducting structure in the study area; the primary water-conducting channels are the fracture zones formed during coal extraction. Based on our previous in-situ monitoring and predictive analysis (Zeng et al. 2023), the water-conducting fractured zones formed during the extraction of the 2–2 coal seam will extend into the weathered bedrock aquifer.

(2) Sources of water-inflow: the direct sources of water inflow within the water-conducting fracture zone include the bedrock aquifer and the weathered bedrock aquifer. The bedrock aquifer exhibits low water abundance and negligible lateral recharge. Consequently, when the static storage of this aquifer comes into contact with the water-conducting fractures, it rapidly flows into the mine and subsequently gets drained, leaving the bedrock segment primarily functioning as a conduit during the entire period of mine water inflow. On the other hand, the weathered bedrock aquifer is abundant in water and receives ample lateral recharge, making it the principal source of water inflow for the mine. Additionally, outside the scope of the water-conducting fracture zone, the indirect source of water inflow is the Quaternary groundwater aquifer. Due to sediment wedge disappearance at the western margin of the mine (Fig. 1c), there exists a possibility of vertical recharge to the weathered bedrock aquifer through the presence of the red clay aquitard.

(3) Water-inflow intensity: the distribution of water inflow from different working faces in the mine has revealed differences between the eastern and western panels. In the past, the average water inflow at the 122,108 working face in the eastern panel was 300 m^3/h. As the working face advanced, the water inflow increased accordingly. When the water-conducting fractures came into contact with heterogeneous water-rich zones, the water inflow showed a sudden increase. After the completion of mining at the working face, the water inflow decreased to 200 m^3/h (Fig. 2a). The maximum water inflow at the 122,109 working face in the western panel reached up to 950 m^3/h, and it remained above 600 m^3/h even after mining was completed (Fig. 2b). It can be inferred that the aquifer in the bedrock has a limited capacity to provide water inflow. Due to the presence

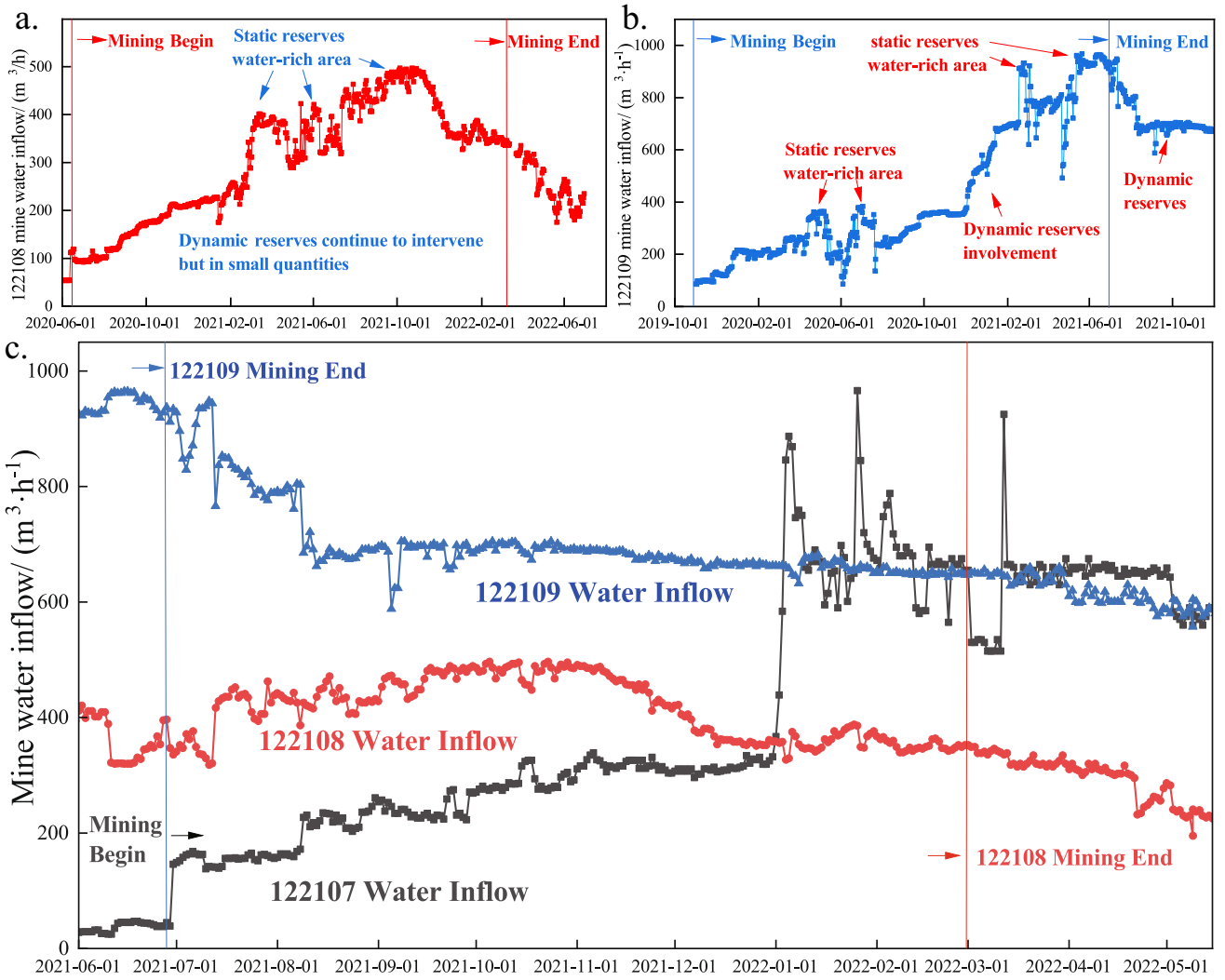

Fig.2 Time series curve of water inflow at each working face (**a** Time series curve of water inflow throughout the entire mining process at 122,108 working face. **b** Time series curve of water inflow throughout the entire mining process at 122,109 working face)

of an impermeable skylight in the western part of the mining area, the Quaternary aquifer indirectly replenishes the weathered bedrock, causing abnormally high water inflow at the 122,109 and 122,107 working faces (Fig. 2c).

Methods

Monitoring of Groundwater Flow Based on Particle-Magnetic Heading Optical Tracking Technology (PMHOTT)

Basic Principle of PMHOTT

For highly heterogeneous fractured aquifers, analysis of the flow field generated from traditional interpolation of GWL monitoring well data may not be sufficiently accurate due to the limited number of monitoring wells. Additionally, in mining areas, GWL monitoring wells are typically not installed above the mining working faces to prevent the formation of preferential flow paths. This limitation hampers a precise understanding of the flow field variations in the areas most affected by coal mining. Therefore, in this study, we used the PMHOTT to collect monitoring data on groundwater velocity and flow direction. This allowed us to further analyze the seepage patterns of the groundwater, compensating for the limitations of traditional flow field analysis.

PMHOTT utilizes imaging techniques to monitor the movement trajectory of colloidal particles carried in groundwater to determine groundwater velocity and direction (Fig. 3). The natural particles and colloids that exist in groundwater possess neutral buoyancy. PMHOTT employs a high-resolution electronic compass, a high-magnification particle-imaging camera, and precise capture software to monitor the flow velocity and direction. When colloidal particles in groundwater pass through the imaging area of the instrument, they are observed and monitored, thereby providing information on groundwater velocity and direction. The instrument captures highly magnified images of suspended colloidal particles within the groundwater well and provides accurate magnetic heading information. By digitizing and analyzing these images, the movement trajectory of colloidal particles can be determined. By incorporating compass data, the flow direction of each colloidal particle can be determined, while the horizontal velocity of the particles (i.e. flow velocity) is being automatically calculated. To obtain reliable results, in practical operations, it is typically necessary to monitor continuously for at least 15 min to acquire a large amount of particle data. Based on the average values derived from this data, the final groundwater velocity and direction can be determined.

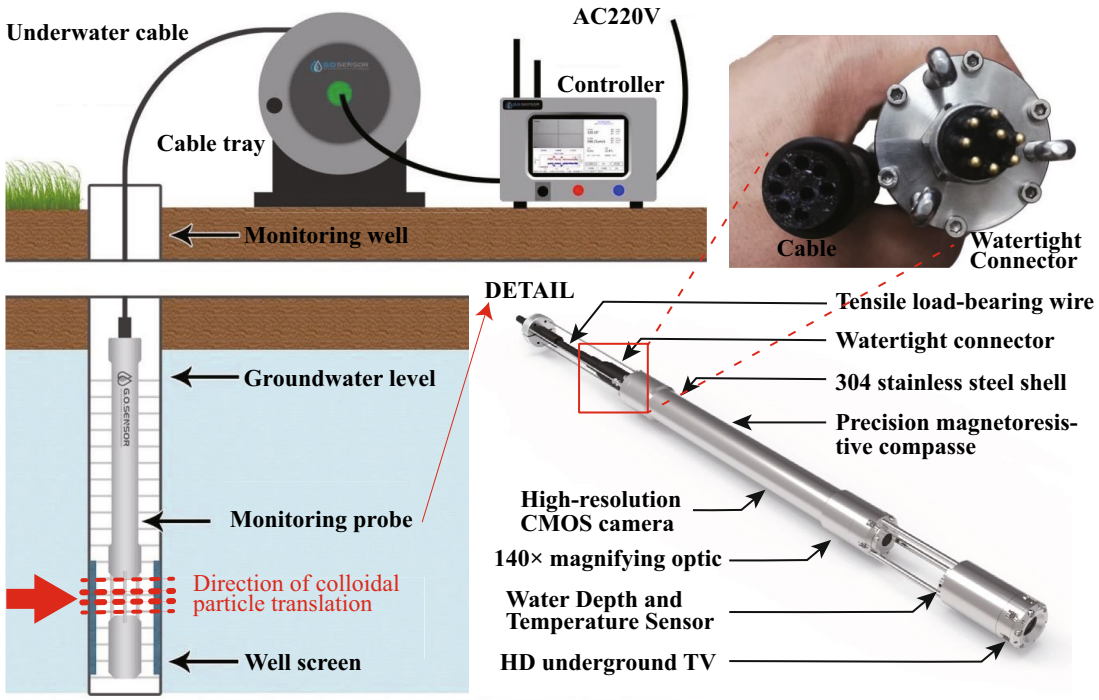

Fig. 3 Schematic diagram of PMHOTT

Calculation of the Hydraulic Conductivity

Due to the differing hydraulic conditions between aquifers and wells, groundwater flow typically exhibits converging flow lines towards wells (Cook et al. 2010). Due to the hydraulic contrast between the aquifer and the well, the flow velocity in the well (referred to as v_{ww}) can be much higher than the groundwater flow velocity in the main aquifer (referred to as v_{gw}). Several methods have been developed to quantify this effect (Schubert et al. 2011). Drost et al. (1968) discovered an empirical relationship between inflow width and well radius and introduced a horizontal convergence factor based on well geometry and all relevant hydraulic conductivity data (Eq. 2). Through application, the groundwater flow velocity in the undisturbed aquifer (v_{gw}) can be quantitatively related to the determined velocity inside the well (v_{ww}) using Eq. 1:

$$v_{gw} = v_{ww}/\alpha \tag{1}$$

If the well is constructed without any filter pack, or if the hydraulic conductivity of the filter pack can be assumed to be equal to the hydraulic conductivity of the aquifer, the convergence factor α can be expressed by Eq. 2:

$$\alpha = \frac{4}{1 + \left(\frac{r_w}{r_s}\right)^2 + \left(\frac{K_2}{K_1}\right)\left[1 - \left(\frac{r_w}{r_s}\right)^2\right]} \tag{2}$$

If no skin effect is considered (r_w=r_s and K_2=K_1), Eq. 2 can be simplified to α=2, which was developed and published empirically by Ogilvi and applied by Cook et al. (1999). Equation 3 can thus be used to quantify the relationship between the well velocity and the aquifer flow velocity.

$$v_{gw} = v_{ww}/2 \tag{3}$$

where v_{gw} is the groundwater flow velocity in the aquifer (L/T), v_{ww} is the groundwater flow velocity in the well (L/T), α is the horizontal convergence factor, r_s is the skin zone radius (L), r_w is the well radius (L), K_1 is the the hydraulic conductivity of the skin zone (L/T), and K_2 is the hydraulic conductivity of the aquifer (L/T).

By monitoring the flow velocity in the well (v_{ww}) and utilizing Eq. 3 to convert it into aquifer flow velocity (v_{gw}), the hydraulic conductivity of the aquifer (K_2) can be calculated using Darcy's Law (Eq. 4). This process allows for a more comprehensive understanding of the heterogeneous characteristics of the aquifer, facilitating quantitative calculations of groundwater seepage times.

$$v_{gw} = K_2 I = K_2 \frac{\Delta H}{\Delta L} \tag{4}$$

where I is the hydraulic gradient, ΔH is the difference in GWL between two points (L), and ΔL is the horizontal distance between the two points (L).

Tracer Based Vertical Seepage Monitoring of Groundwater

Artificial tracer tests are methods in which substances that can move with groundwater and are not easily adsorbed are injected into a specific part of a groundwater system, and their movement is monitored and detected elsewhere. This technique has been widely applied for reasons such as water source exploration in karst regions (Kogovsek and Petric 2014), dam leakage detection (Qiu et al. 2022), pollution source tracking (Schiperski et al. 2022), and tunnel disaster prevention (He et al. 2023). In the mining field, artificial tracers are used for the examination of hydrodynamics and calculation of mean residence times, particularly in the hydrological processes pertaining to mine water treatment or abandoned mines (Wolkersdorfer et al. 2016). In the aforementioned scenarios, the presence of relatively continuous or well-connected seepage passageways prevails, which simplifies the determination of tracer injection and monitoring sites for the conducted tests. However, in groundwater systems that have been disturbed by mining activities, the development of water-conducting fractures often exhibits marked heterogeneity. So, for example, such characteristics can cause the tracer to be rapidly released from the mining fracture into an isolated water-rich space, thus preventing it from reaching the mine. When compared to the flow within these fractures, the flow capacity of the bedrock seems relatively limited. This heterogeneity presents a considerable challenge for tracer injection. Therefore, conducting artificial tracer experiments in mining areas with fractures developed in the coal roof in northwest China has important pioneering value and guiding significance for the application and promotion of this technology. In addition, plotting the concentration–time curve of the tracer and analyzing its characteristics provides a new means to further explore the hydraulic connection between different aquifers in the overburden of the roof and determine the nature of groundwater flow when roof failure occurs.

Basic Principle of Artificial Tracer Tests

When a tracer is injected into groundwater, it does not move forward at the actual flow velocity but spreads and propagates continuously with the fluid flow (Hinton and Woods 2019). It expands within the fluid and extends beyond the region influenced solely by the average flow velocity. This phenomenon is called hydrodynamic dispersion, which is an unstable and irreversible process. During the flow and diffusion of the tracer, the concentration of the tracer varies over time. By establishing hydrodynamic

dispersion equations for different media, corresponding breakthrough curves can be solved, thus establishing the relationship between the media and the tracer curve patterns.

Within heterogeneous aquifers, tracers migrate faster in permeable media, resulting in larger dispersion plumes. Therefore, tracer tests always directly reflect the characteristics of high conductivity zones and hydrodynamics in the aquifer, where groundwater flow velocities are high. Consequently, when studying the flow of tracers, molecular diffusion can be neglected, and only mechanical dispersion is considered (Brouyere 2003). The fundamental one-dimensional advection–dispersion equation for such cases is given as:

$$\frac{\partial C}{\partial t} = D\frac{\partial^2 C}{\partial^2 x^2} - V\frac{\partial C}{\partial x} \tag{5}$$

where C represents the tracer concentration, t is time, x is distance, and D is the dispersion coefficient that describes the rate at which the tracer disperses in the medium. This equation describes the relationship between the tracer concentration and changes in time and space. By solving this equation, we can obtain the distribution of tracer concentration over time and space. As shown in Eq. 5, the changes in tracer concentration with time is related to the dispersion coefficient and groundwater flow velocity.

In addition, when the working face of a coal seam is mined to a certain length, it disrupts the original stress equilibrium of the overlying strata of the goaf, leading to phenomena such as collapse, movement, deformation, and detachment of the overlying strata. Based on the degree of fragmentation, different zones are formed from top to bottom, including bending and sinking zones, fracture zones, and caving zones. Well-developed fracture and caving zones can form effective water-conducting channels. By using stable, soluble tracers, and taking advantage of dispersion within the aquifer, the tracers can migrate within the water-conducting channels formed by the overlying strata damage, and eventually reach the inflow point in the working face. By monitoring the tracer concentration in water samples collected from the corresponding inflow in the working face and analyzing how it changes over time, the source and movement patterns of the water inflow can be determined.

This study employed a fluorometer for continuous and automated monitoring during the tracer experiment. The optical component consists of lights with different frequencies located on four vertical axes (Fig. 4a). Each axis is equipped with excitation point filters, detection point filters, and optical lenses. As water flows through the optical aperture, these lights are sequentially turned on and off to measure three independent responses and the turbidity of the water (Pecly 2018).

Artificial Tracer Test

According to the research objectives, experimental principles, and field survey measurements, we selected three fluorescent tracers, namely uranine, rhodamine, and tinopal, for our experiment. Compared to other tracers like sodium chloride and ammonium molybdate, fluorescent tracers have the advantages of stability, low dosage, high detection accuracy, and continuous monitoring capability. To ensure the reliability and accuracy of the field test data, two sets of indoor calibration experiments were conducted. The first set of experiments determined the relationship between the tracer concentration and detection results. By adding an equal amount of tracer and continuously measuring the results, a linear correlation between the two indicates normal instrument function. The second set of experiments determined the instrument's detection threshold and whether there would be interference between the three tracers. The three types of tracers were added in sequence to the same container, and the results were judged based on the detection results.

To improve the accuracy and success rate of the experiment, the modified flow field and PMHOTT were adopted to precisely delineate the central area of the cone of depression and determine the injection location of the tracer. A double-plug water pressure device was used to inject pre-prepared proportional tracer reagents into designated boreholes. After entering the water-bearing layers, the tracers flow into the goaf area through water-conducting fissures. Monitoring points were set near the corresponding goaf areas, and by measuring the concentration changes of the tracers, we could understand the effective height of the development of water-conducting fissure zones in the overlying rock strata, as well as the timing and range of groundwater inflow from different aquifers into the working face. In this study, we injected the three tracers into the Salawusu Formation, weathered bedrock, and Zhiluo Formation aquifers respectively, as shown in Fig. 4c and Table 1. Monitoring devices were placed at the water tank of the auxiliary transportation groove of the 122,107 working face at a distance of 4700 m (Fig. 4e). The monitoring data allowed us to study the movement characteristics of the groundwater in the mining-influenced overburden and provided support for subsequent anti-seepage or grouting sealing measures.

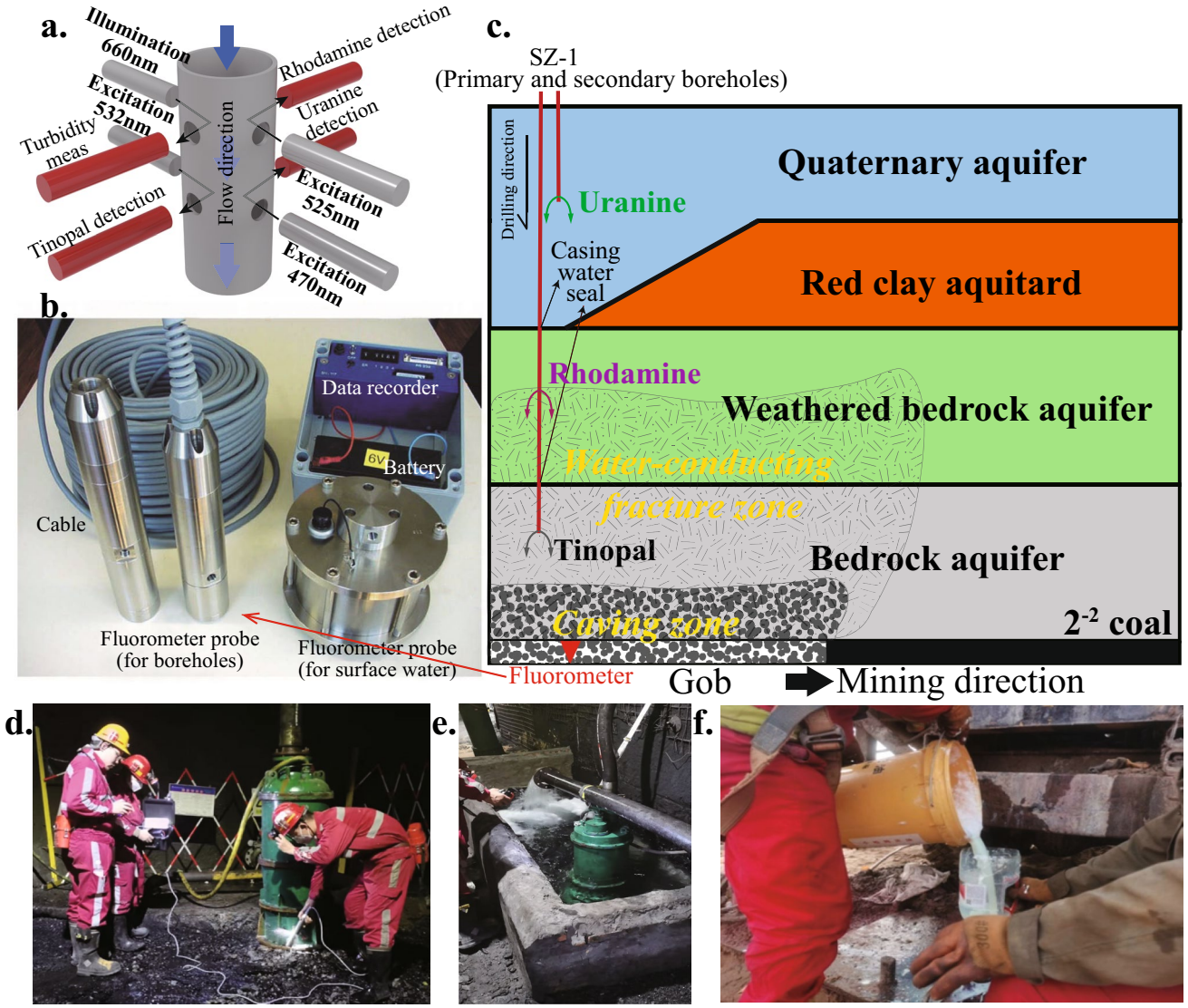

Fig. 4 Principle of tracer equipment and test schematic (**a** Schematic of fluorometer principle, **b** Physical fluorometer, **c** Tracer test scheme, **d** Background value measurement of downhole tracer test, **e** Water tank for continuous monitoring at the working face, **f** Ground borehole to inject tracer)

Table 1 Summary of tracer experiment arrangement in each aquifer

ID	Time	Inject aquifer and depth	Tracer and its dosage	Inject position	Monitoring position
1	2022/3/10 13:00	Weathered bedrock 83.5m	Rhodamine 3kg	Borehole SZ-1	The water tank of the auxiliary transportation groove of the 122,107 working face at a distance of 4700 m
	2022/3/11 15:15	Weathered bedrock 84.2m	Rhodamine 3kg		
	2022/3/11 17:40	Weathered bedrock 88.2m	Rhodamine 3kg		
	2022/3/12 11:30	Weathered bedrock 115.6m	Rhodamine 5kg		
	2022/3/17 10:30	Weathered bedrock 84m	Rhodamine 5kg		
2	2022/3/27 9:00	Zhiluo 181m	Tinopal 10kg		
3	2022/3/30 12:00	Salawusu 32.5m	Uranine 10kg	Pair borehole SZ-1	

Results

Groundwater Horizontal Flow

Weathered Bedrock Aquifer

Through analysis of the water-filling factors in the mine, we found that the weathered bedrock aquifer was the main source of the water inflow. Understanding the flow field distribution in the weathered bedrock is crucial for preventing and managing water hazards. In order to accurately obtain the GWL seepage patterns in the weathered bedrock aquifer, we utilized GWL monitoring data from March 2022 and flow velocity and direction data obtained from PMHOTT to generate a flow field. The interpolated flow field generated by direct interpolation with the corrected flow field incorporating flow direction data is shown in Fig. 5. It can be observed that the weathered bedrock forms two descending funnels. One stable funnel was formed after mining of the 122,109 working face was completed. Another new funnel gradually formed when mining at the 122,107 working face began, with its influence range gradually expanding as mining progressed.

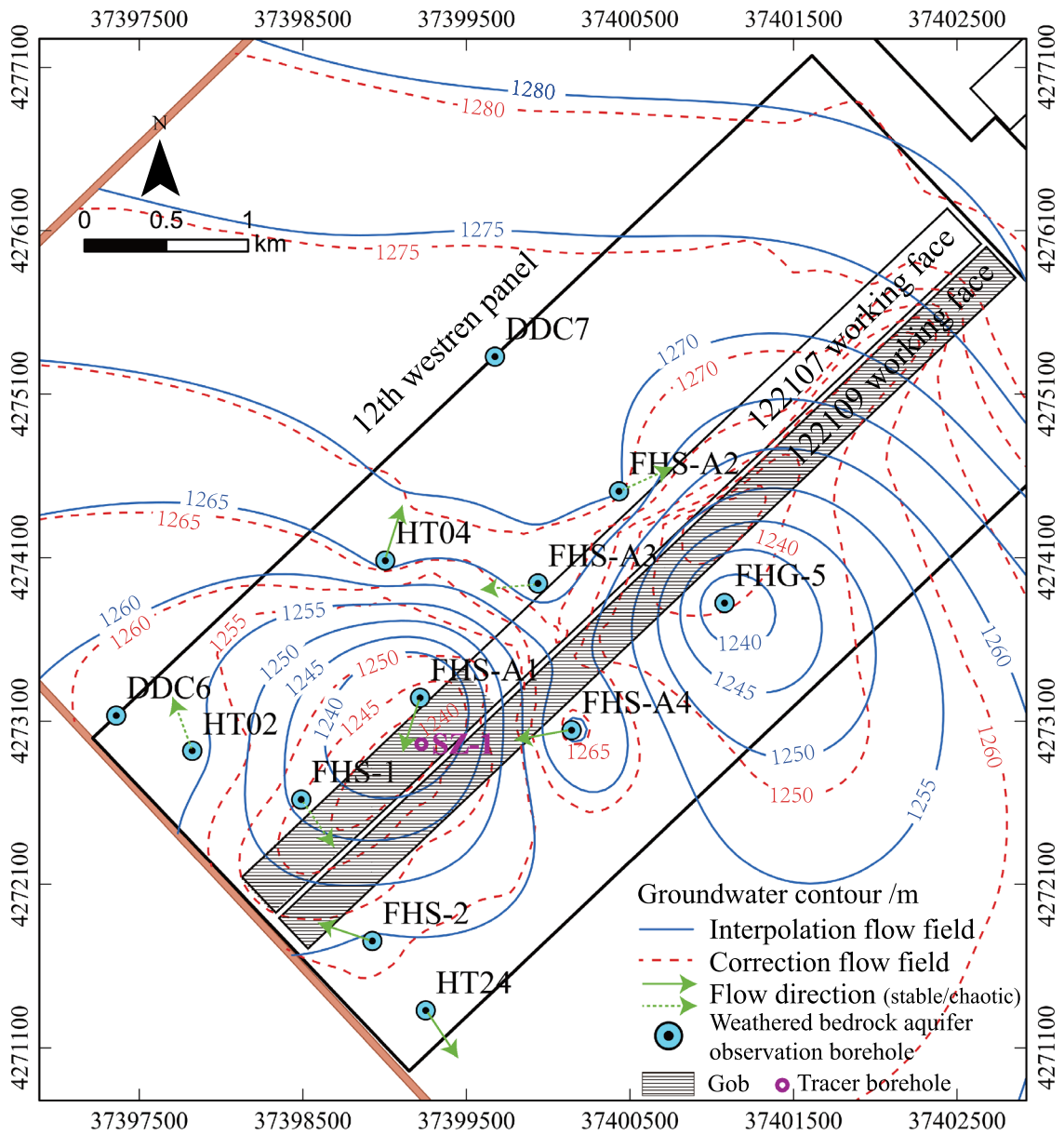

Fig. 5 Contrast of direct interpolated flow field with corrected flow field in weathered bedrock aquifer

Furthermore, the corrected flow field centers on the working face, providing a more realistic representation of the flow field in the weathered bedrock and compensating for the drawback of not being able to install GWL monitoring boreholes above the mining face. This correction allowed us to have a more accurate understanding of the water flow dynamics in the weathered bedrock, providing a more reliable reference for the prevention and management of mine water inflow (Fig. 6).

Quaternary Aquifer

By observing the flow field morphology generated by GWL interpolation, we identified a macroscopic trend of northeast to southwest groundwater flow in the Quaternary aquifer. However, as the borehole monitoring was conducted closer to the working face, we observed that the groundwater flow direction differed from the macroscopic trend, resembling that of the weathered bedrock aquifer. This suggests that under the influence of mining, groundwater started to converge towards the goaf area. The corrected flow field morphology is generally similar to the interpolated flow field morphology, except for the relatively lower GWL near the working face. This is due to the effects of mining on the groundwater system, resulting in relatively lower GWL near the working face.

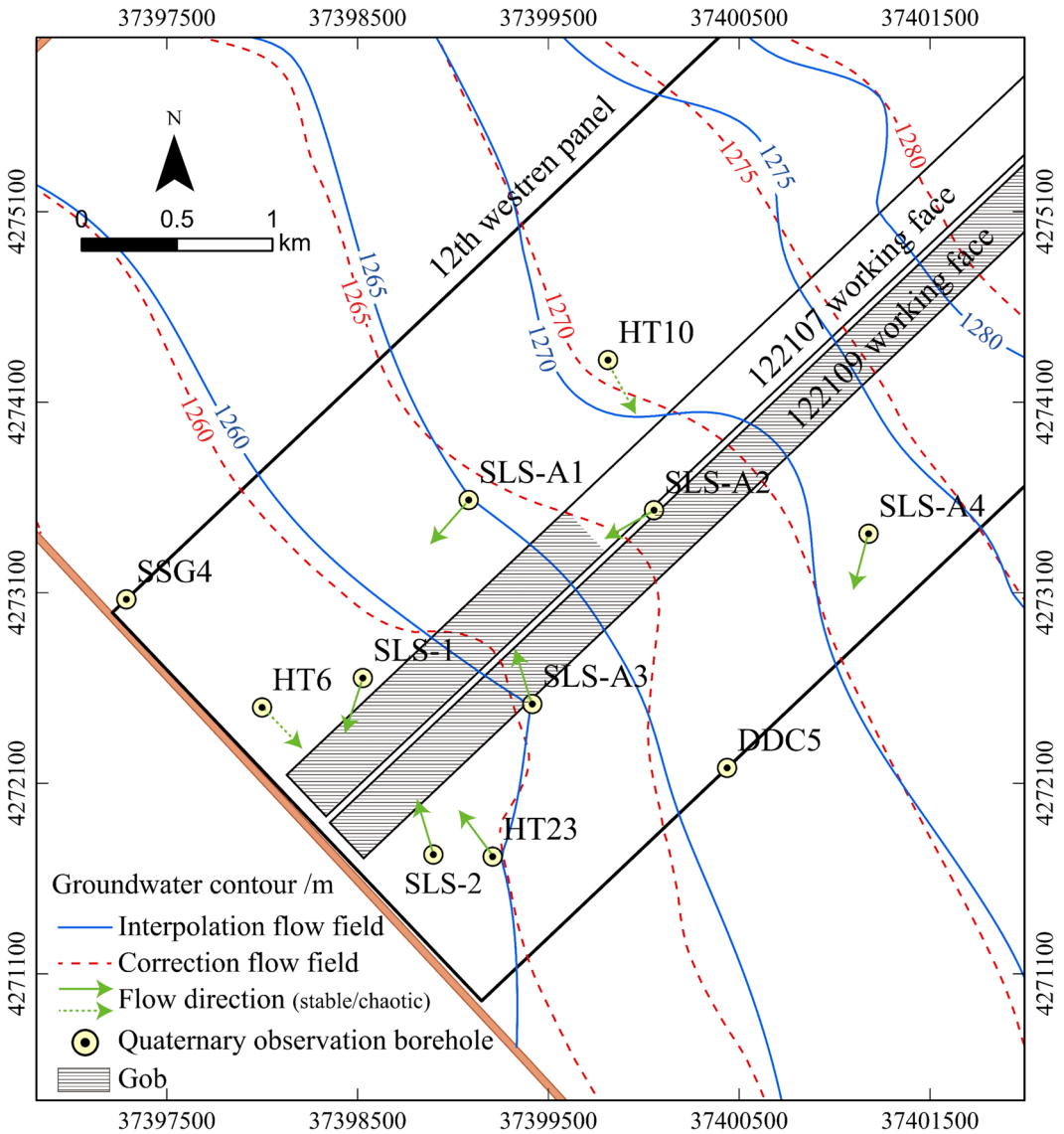

Fig. 6 Contrast of direct interpolated flow field with corrected flow field in Quaternary aquifer

Groundwater Vertical Tracer Results

Laboratory Test To ensure the reliability and accuracy of the field test data, we conducted indoor calibration experiments for tracer analysis. Prior to the calibration experiments, measurements and calibrations were performed on the tracers used. Specifically, we used tracer standard solutions to detect and analyze the relationship between the instrument-measured concentration and the true concentration (Fig. 7). From Fig. 7, it can be observed that the true concentrations of the three tracers can all be represented by a linear equation "$y = kx + b$" with their measured concentrations. In this equation, y represents the measured concentration, and x represents the true concentration. The results showed that the coefficient of determination (R^2) for all three tracers exceeded 0.98, indicating that the tracer instruments used were accurate and reliable, and correlated well with the actual concentrations.

To avoid potential interference from outliers in the field experiments, we conducted indoor experiments using cross-detection of tracer reagents to clarify the detection status and abnormal conditions of the tracer device under different circumstances. The specific procedure involved sequentially adding the three fixed-concentration tracer reagents into the water and recording the concentration changes while observing the changes in the detected concentrations of the other two sets of tracer reagents (Fig. 8). The experiment was conducted in four phases. The results showed that in phases 1 ~ 2, when the uranine and rhodamine were individually added at a concentration less than 250.00 ppb, their influence on the detected concentrations of the other two sets of tracer reagents was negligible and could be ignored. However, after adding the fluorescent whitening agent, the detected concentration of rhodamine and the turbidity of the liquid both decreased in phase 3; the decrease in the detected concentration of the uranine was less than the decrease in the turbidity of the liquid. When the concentration of the fluorescent whitening agent exceeded 150.00 ppb and continued to increase, the detected concentration of rhodamine similarly increased. As the concentration of tinopal was increased, when it reached ≈ 813.00 ppb, the reading of the detection device no longer changed; the concentration readings of the three tracer reagents had reached their upper detection limit. Furthermore, due to the differences in the optical properties of the three tracer reagents, the turbidity value in the detection solution was positively correlated with the detected concentrations of uranine and rhodamine, but negatively correlated with the detected concentration of the fluorescent whitening agent. Through these indoor experiments, we were able to gain a better understanding of the interactions and optical characteristics among the three tracer reagents, as well as their potential interference with the detection results. This enabled us to analyze and interpret the data in the field experiments and improve our understanding of groundwater flow behavior.

In situ Tracer Test Before conducting the tracer test, we performed indoor testing and field background value tests on the

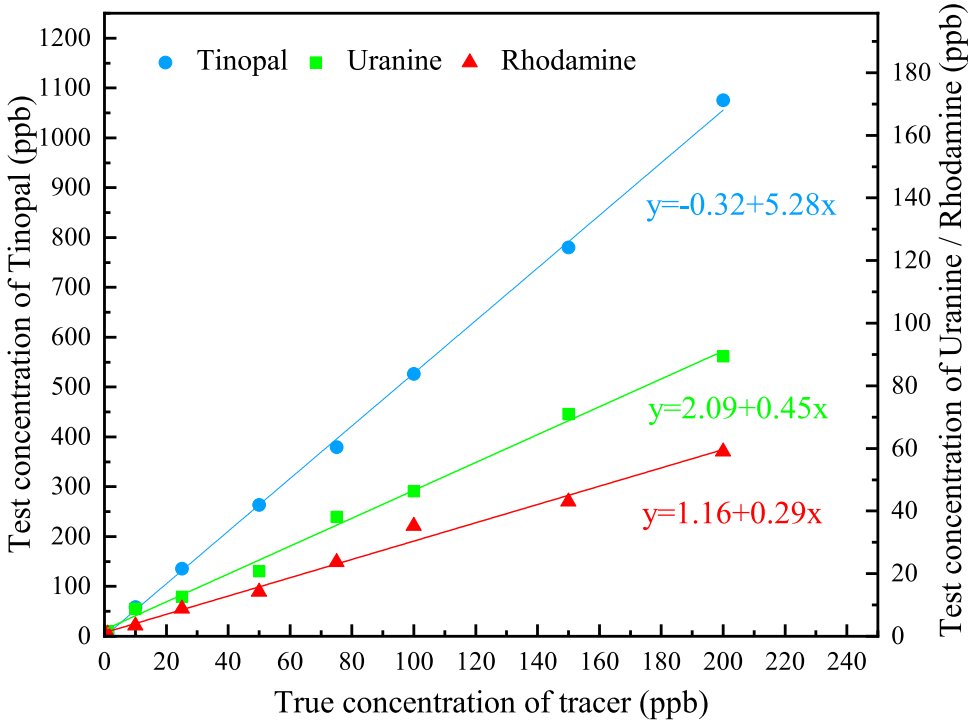

Fig. 7 Regression analysis of true tracer concentration and monitored concentration

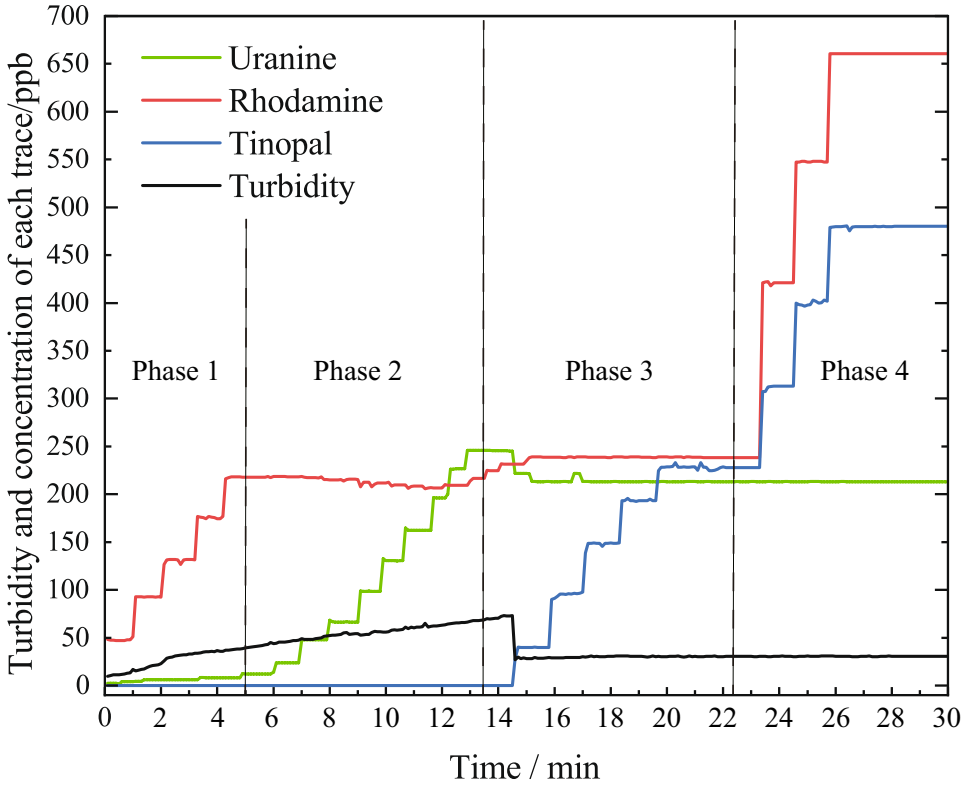

Fig. 8 Laboratory cross test of each tracer

automatic monitoring device to minimize potential errors and problems. As shown in Fig. 4d, background measurements were taken at the tracer injection points and detection points, and the amount of tracer was estimated based on the estimated catchment area and length of the flow path. Additionally, due to the potential influence of tinopal by human activities (Hayakawa et al. 2007), it was essential to ensure that the background values near the receiving points were within an acceptable range before using the pre-designed and prepared tracers.

Therefore, for this tracer test, based on the hydrogeological conditions of different aquifers and the actual field situation, SZ-1 main and secondary boreholes were selected as inject points (Fig. 5). A total of 19 kg of rhodamine tracer was sequentially injected into the weathered bedrock aquifer, 10 kg of tinopal was injected into the Zhiluo Formation fractured aquifer, and 10 kg of uranine was injected into the Salawusu Formation confined aquifer (Table 1). The test receiving point was the sealed water tank in the auxiliary transportation haulage 4700 m from the 122,107 working face. The monitored tracer concentrations at the receiving point are shown in Figs. 9 and 10.

(1) According to the monitoring curves of the tracer concentration at the underground receiving point from March 10th to March 12th, 2022 (Fig. 9a), the following observations were made: on March 10th at 13:00, we injected 3 kg of rhodamine tracer into the weathered bedrock section at a depth of 83.5 m. On March 11th at 10:30, a slight increase in rhodamine concentration was observed. At that time, the background concentration range for rhodamine was 1.61–6.67 ppb, and the increase range was 9.11–15.91 ppb, with a duration of 11.25 h. On March 11th at 15:15 and 17:40, we respectively injected 3 kg of rhodamine tracer at depths of 84.2 and 88.2 m. On March 12th at 2:46 and 7:46, the rhodamine concentration showed two-stage increases. The first stage had an increase range of 18.63–20.68 ppb, with a duration of 3.75 h. The second stage had an increase range of 10.21–31.84 ppb, with a duration of 2.25 h.

As shown in Fig. 9b, the following observations were made: At 10:30 on March 17th, we injected 5 kg of tracer into the weathered bedrock section at a depth of 84 m. On March 19th at 13:36, an increase in rhodamine concentration was observed. At this time, the background concentration of rhodamine ranged from 1.82 to 3.05 ppb, with the increase ranging from 9.32 to 15.28 ppb and a duration of 1.16 h.

From March 24th to April 17th, 2022 (Fig. 10a), the following observations were made: on March 26th at 20:25, the rhodamine concentration exceeded the maximum background value and showed an upward trend. After the concentration reached 34.61 ppb, it began to slowly decrease. As the concentration decreased to 29.97 ppb, the rate of decrease increased until it returned to the background value. The entire process of change lasted for 417 h.

(2) The second group of Zhiluo Formation bedrock aquifer tracer monitoring results was from March 24th to April 17th, 2022 (Fig. 10b). On March 27th at 9:00, we injected 10 kg of

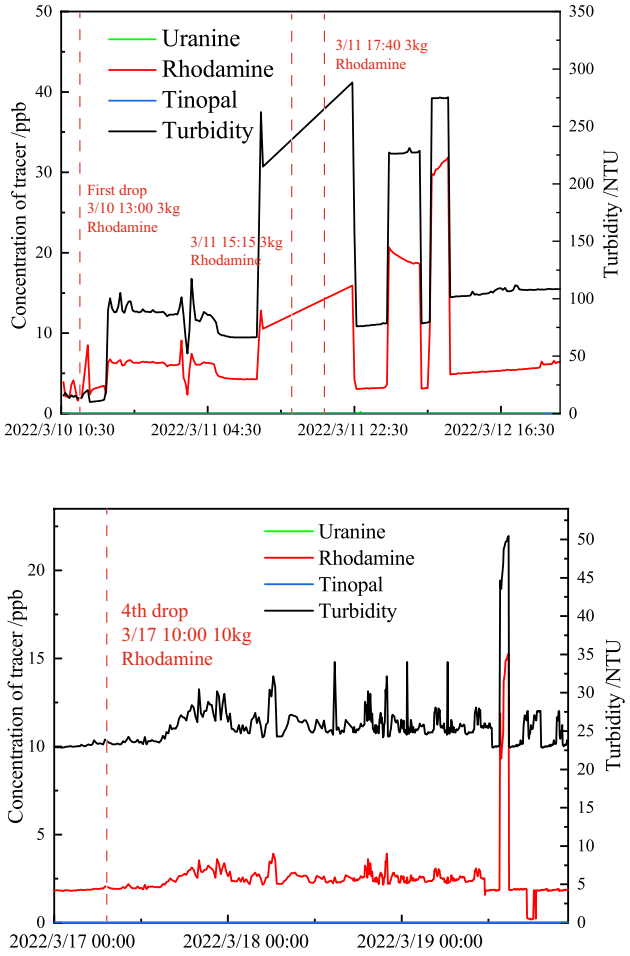

Fig. 9 The first group of weathering bedrock aquifer tracer monitoring results

Tinopal into the fractured aquifer section at a depth of 181 m. At 14:31 on March 27th, an upward trend was observed in the concentration curve of the fluorescent whitening agent. The increase was followed by a decrease, eventually disappearing. The maximum value was 4.90 ppb, over 55.25 h.

(3) The third group of Quaternary aquifer tracer monitoring results was from March 24th to April 17th, 2022 (Fig. 10c). On April 4th at 12:00, 10 kg of uranine were injected into the confined aquifer section of the Salawusu Formation at a depth of 32.5 m. On April 14th at 21:41, a change was observed in the concentration curve of uranine, with a sharp increase followed by a rapid decrease, eventually disappearing. The range of change was between 1.07 and 1.85 ppb, over 13.92 h.

Discussion

Analysis of Groundwater Horizontal Seepage

Based on the corresponding relationship between the morphology and flow direction in Fig. 5, boreholes FHS-1, FHS-2, and FHS-A2 show a tendency to flow towards the center of the funnel, but they do not fully align with the direction of hydraulic gradient. Additionally, HT02, HT04, and HT24 have very slow flow velocities, and their flow directions are completely opposite to the macroscopic hydraulic gradient. Therefore, it can be inferred that the flow characteristics of the weathered rock aquifer are highly complex, indicating heterogeneity. The morphology and flow direction of the flow field exhibit certain local variations, which do not fully align with the macroscopic hydraulic gradient. Furthermore, the influence range of the cone of depression formed by extraction is limited.

The comparative monitoring data is shown in Table 2. The hydraulic conductivity coefficients were determined by measuring the groundwater flow rates in the observation wells and then calculated using Eqs. 3 and 4. The hydraulic conductivity in the weathered bedrock aquifer ranged from 1 to 10 m/d. The hydraulic conductivity was 0.085 m/d in a single observation well, FHS-A4. Analysis of the scatter plot (Fig. 11) indicates consistently low flow rates, despite continuous changes in flow direction. In addition, a water mound had formed at the location of FHS-A4, where the flow velocity is extremely slow. Moreover, the flow direction changed systematically from pointing towards one funnel center to another, indicating that this may be a groundwater watershed (Georgek et al. 2018). The hydraulic conductivity determined from observation wells in the Quaternary aquifer ranged from 10 to 18 m/d, which is consistent with the pumping test results (Qu et al. 2021a).

When the groundwater flow velocity is low, the flow velocities and directions of different colloidal particles are relatively chaotic and lack uniformity. This may be attributed to the fact that when the groundwater flow velocity is low, the flow is more susceptible to external factors, causing the colloidal particles to experience different forces during their movement, resulting in a more disordered flow velocity and direction (Adinehvand et al. 2020). Additionally, since only groundwater is present within the borehole without any other substances impeding water infiltration, the permeability coefficient calculated using Darcy's law has a relatively high value.

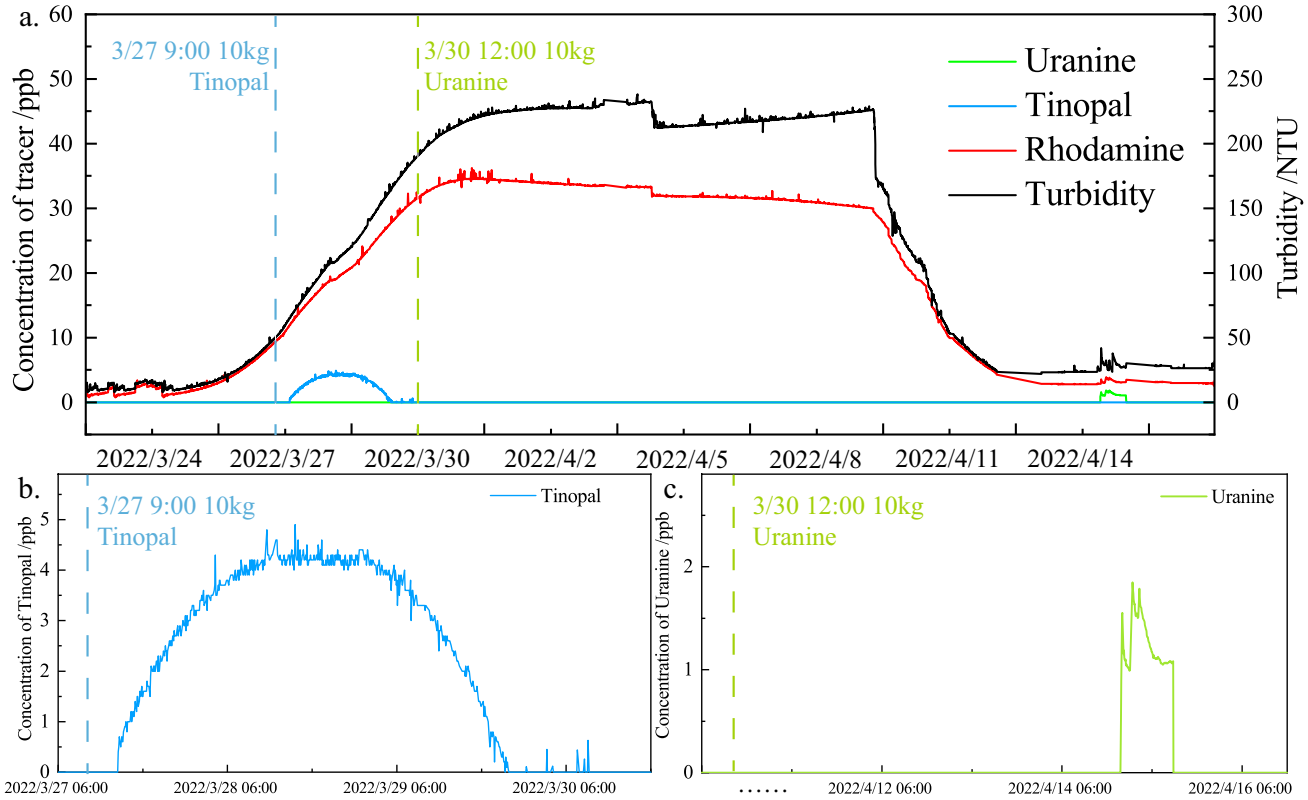

Fig. 10 The second and third group tracer monitoring results

Table 2 Monitoring Data of Flow Velocity and Direction, and Calculated Hydraulic Conductivity (K_2)

Aquifer	ID	Average flow direction/°	Average flow velocity v_{ww}/(m/d)	Hydraulic conductivity K_2/(m/d)	Note
Weathered bedrock	FHS-1	142.1	2.691	4.037	Relatively stable
	FHS-2	288.5	1.729	9.423	Relatively stable
	FHS-A1	197.5	2.515	5.961	Chaotic
	FHS-A2	66.7	0.8583	1.451	Chaotic
	FHS-A3	264.4	0.7571	2.832	Chaotic
	FHS-A4	288.5	0.0519	0.085	Chaotic but continuous
	HT04	17.8	0.8846	2.340	Relatively stable
	HT24	146.3	0.09702	1.941	Chaotic
	SZ-1	99.2	7.7976	6.706	Very chaotic
Quaternary	SLS-1	221.1	1.43	16.159	Stable
	SLS-2	343.4	1.256	7.756	Relatively stable
	HT06	136.3	0.1553	2.163	Chaotic
	HT10	151.6	1.329	13.290	Chaotic
	HT23	323.4	1.761	18.226	Stable
	SLS-A1	221.2	2.474	10.144	Relatively stable
	SLS-A2	304.2	1.659	17.503	Relatively stable
	SLS-A3	343.0	1.254	10.346	Stable
	SLS-A4	194.8	1.787	10.410	Relatively stable

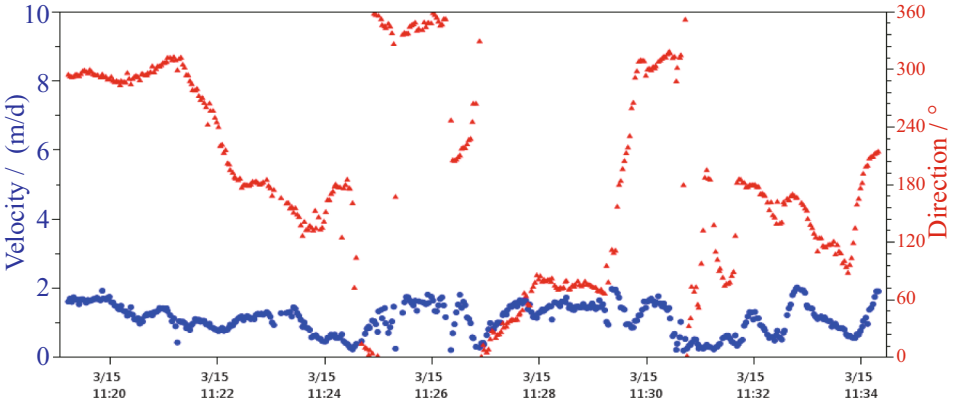

Fig. 11 Scatter plot of velocity and direction in FHS-A4

Analysis of Groundwater Vertical Seepage

The monitoring results of the first tracer group indicate that there may be two ways for the tracers to flow into the mine from the weathered rock aquifer. After the first four tracer injections, a sudden increase in concentration was detected, with durations of 11.25, 3.75, 2.25, and 1.16 h, respectively. These durations were relatively short and had small time spans compared to the injection time. After 391 h, continuous changes in the monitoring concentration were observed, lasting for 417 h. Based on preliminary data such as core identification of the boreholes, it can be inferred that the degree of fracture development in the weathered rock section of the stable formation depends not only on sedimentary environments but also on subsequent mining-induced damage. Both lateral and vertical fractures are well-developed in this rock layer. Therefore, it is possible to divide the groundwater flow in the weathered rock aquifer into two stages. The first stage corresponds to the concentration variations observed after the first four injections. Some tracers rapidly migrated through the vertical fractures (conduit channels) in the weathered bedrock to the monitoring well in the goaf area. The second stage refers to the observations starting from March 24th. The concentration of rhodamine gradually increased, suggesting that the tracer continuously infiltrated vertically into the goaf area after horizontal seepage and diffusion within the weathered rock layer through the lateral fractures. Therefore, it can be concluded that the weathered bedrock aquifer in the stable formation is hydrologically connected not only with the fissured aquifer in the ZhiLuo Formation, but also serves as a direct water source for the mine production process.

The second tracer group consisted of tinopal, which was injected into the fissured aquifer of the Zhiluo Formation. After 5.5 h, a change in tracer concentration was detected underground, with a duration of 55.25 h. Due to the small distance between the Zhi Luo Formation aquifer and the coal seam, as well as marked damage, the development of conduit pathways is more pronounced. This situation favors vertical seepage of the tracers. Therefore, after the tinopal was injected into the fissured aquifer of the Zhiluo Formation, groundwater rapidly passed through the fractured overburden and into the goaf area. This further confirms the high degree of vertical fracture development in the Zhiluo Formation aquifer, making it a direct water source for dewatering during the mining process (Qu et al. 2021b).

The third tracer group consisted of uranine, which was injected into the confined aquifer of the Salawusu Formation. After 249.6 h, a change in tracer concentration was detected underground, with a duration of 13.92 h. Although preliminary data such as geological structures and borehole exposures indicate that under mining-induced damage conditions, the highest development of conduit channels occurs in the weathered bedrock section of the stable formation and does not directly connect to the confined aquifer of the Salawusu Formation, the aquitard between the two aquifers is relatively weak in this area and is also affected by mining-induced damage. Therefore, after the sodium fluorescein tracer entered the weathered rock aquifer, it followed the conduit channels formed by mining-induced damage and flowed into the goaf area. Based on the results of the third tracer experiment, it can be inferred that there is a hydraulic connection between the confined aquifer of the Salawusu Formation and the weathered bedrock aquifer of the stable formation, serving as an indirect water source for the mining face (Zeng et al. 2024).

In summary, the groundwater flow process can be divided into two stages. The first stage is rapid inflow into the mine through the main channel, which enters from the Zhiluo Formation, the weathered bedrock, and the Quaternary aquifer for 2, 48, and 389 h, respectively. The second stage involves entry into the mine with natural diffusion of the tracer and hydraulic exchange between aquifers. In this second stage, the monitoring is limited to the tracers in the weathered bedrock. It is hypothesized that the tracers of the Zhiluo

Formation all entered the mine in the first stage. Tracers from the Quaternary aquifer flowed into the mine after a long period of time, resulting in very low concentrations that made monitoring during the second phase challenging.

Limitations of Tracer Tests in Fractured Aquifers

Tracer tests in karst groundwater systems and subterranean rivers are highly effective in accurately understanding the seepage characteristics of groundwater, providing advantages in both temporal and spatial aspects (Peely et al. 2021). However, there are limitations when conducting such tests in fractured aquifers. To address these limitations, we made thorough preparations in the preliminary stage and additionally set up an injection well. The experimental results show that the method worked well in vertically developed fractures with good hydraulic conductivity. However, when we conducted experiments in hydrological monitoring wells located ≈ 1 km from the injection well horizontally, we did not obtain effective monitoring results. One possible reason is that the transport time of groundwater was too long relative to our monitoring period. Another more important factor is the heterogeneity of fractured aquifers, which can unexpectedly divert the tracer-laden groundwater to different locations (Sommer et al. 2013).

It is essential to accurately grasp the true development height and conditions of water-conducting fracture zones during coal mining operations. This study, as a low-cost monitoring method, utilized on-site borehole investigations. It not only enables a more accurate determination of the development height of water-conducting fracture zones but also provides quantitative information about the seepage time and patterns of groundwater. Mining personnel can conduct subsequent mining activities more effectively and safely, based on the aforementioned information.

Conclusions

Fractured aquifers are typically non-homogeneous, making it challenging to study the sources and paths of mine water inflow using artificial tracer tests, which otherwise have the advantage of being very intuitive. In this study, a combination of PMHOTT and artificial tracer technique allowed us to successfully monitor groundwater inflow from multiple aquifers into a mine. The flow field was measured using PMHOTT to determine the velocity and direction of horizontal groundwater flow, which was then corrected to accurately identify the distributional characteristics of the groundwater flow cones affected by mining activities. Tracers were subsequently injected at the flow cone center, and the vertical seepage characteristics of groundwater were determined by real-time monitoring in the mine.

The results of the study showed that the corrected flow field, measured using PMHOTT, overcame the limitations of traditional methods that lacked sufficient observation boreholes for long-term water level monitoring. This approach accurately captured changes in the flow field in the areas primarily affected by mining activities. Additionally, the hydraulic conductivity coefficient of the aquifer was determined by quantifying the relationship between the flow rate in the wells and aquifers. The Quaternary and weathered bedrock aquifers had hydraulic conductivity coefficients ranging from 10 ~ 18 to 1 ~ 10 m/d, respectively.

The tracer tests revealed that the mine receives groundwater inflow from all three aquifers located above the coal seam. This inflow process unfolds in two stages: initially, water swiftly enters the mine via the primary channel, infiltrating from the Zhiluo Formation, weathered bedrock, and Quaternary aquifer within 2, 48, and 389 h, correspondingly. Subsequently, the second stage involves natural diffusion of the tracer and hydraulic exchange between aquifers as it enters the mine.

In conclusion, this methodology reduced uncertainties associated with traditional methods and expands the applicability of artificial tracer experiments in fractured aquifers. Furthermore, the approach can help predict and prevent mine water disasters at sites with hydrogeologically complex conditions.

Acknowledgements This research was financially supported by the China National Natural Science Foundation (42027801, 42072284, 42372297), the National Key R&D Program of China (2023YFC3012102, 2021YFC2902004), and the Fundamental Research Funds for the Central Universities (2023ZKPYSH01). The authors also thank the editor and reviewers for their constructive suggestions.

Data availability The data supporting the findings of this study are available from the corresponding author upon reasonable request.

References

Adinehvand R, Raeisi E, Hartmann A (2020) An integrated hydrogeological approach to evaluate the leakage potential from a complex and fractured karst aquifer, example of Abolabbas Dam (Iran). Environ Earth Sci 79:19. https://doi.org/10.1007/s12665-020-09244-4

Brouyere S (2003) Modeling tracer injection and well-aquifer interactions: a new mathematical and numerical approach. Water Resour Res 39:5. https://doi.org/10.1029/2002wr001813

Burnett WC, Peterson RN, Santos IR, Hicks RW (2010) Use of automated radon measurements for rapid assessment of groundwater flow into Florida streams. J Hydrol 380:298–304. https://doi.org/10.1016/j.jhydrol.2009.11.005

Cheng X, Qiao W, Li L, Jiang C, Ni L (2020) Model of mining-induced fracture stress-seepage coupling in coal seam over-burden and prediction of mine inflow. J China Coal Soc 45(08):2890–2900. https://doi.org/10.13225/j.cnki.jccs.2019.0651. (**in Chinese**)

Cook PG, Love AJ, Dighton JC (2010) Inferring ground water flow in fractured rock from dissolved radon. Ground Water 37:606–610. https://doi.org/10.1111/j.1745-6584.1999.tb01148.x

Georgek JL, Solomon DK, Heilweil VM, Miller MP (2018) Using tracer-derived groundwater transit times to assess storage within a high-elevation watershed of the upper Colorado River Basin, USA. Hydrogeol J 26:467–480. https://doi.org/10.1007/s10040-017-1655-4

Hayakawa K, Okumura R, Yamamoto H, Fujiwara M, Yamaji N, Takada H, Kanematsu M, Shimizu Y (2007) Distribution and fluxes of fluorescent whitening agents discharged from domestic wastewater into small rivers with seasonal changes of flow rates. Limnology 8(3):251–259. https://doi.org/10.1007/s10201-007-0220-6

He XD, Li PY, Shi H, Xiao YX, Guo YA, Zhao HH (2022) Identifying strontium sources of flowback fluid and groundwater pollution using Sr-87/Sr-86 and geochemical model in Sulige gasfield. China Chemosphere 306:14. https://doi.org/10.1016/j.chemosphere.2022.135594

He YZ, Wang HX, Zhou J, Su HF, Luo L, Zhang B (2023) water inrush mechanism and treatment measures in Huali Highway Banyanzi Tunnel – a case study. Water 15:22. https://doi.org/10.3390/w15030551

Hinton EM, Woods AW (2019) The effect of vertically varying permeability on tracer dispersion. J Fluid Mech 860:384–407. https://doi.org/10.1017/jfm.2018.891

Kogovsek J, Petric M (2014) Solute transport processes in a karst vadose zone characterized by long-term tracer tests (the cave system of Postojnska Jama, Slovenia). J Hydrol 519:1205–1213. https://doi.org/10.1016/j.jhydrol.2014.08.047

Lai XP, Dai JJ, Xu HD, Chen XZ (2021) Multifield environmental analysis and hazards prevention of steeply inclined deep coal mining. Adv Civ Eng 2021:12. https://doi.org/10.1155/2021/6651088

Laurent J, Bois P, Nuel M, Wanko A (2015) Systemic models of full-scale surface flow treatment wetlands: determination by application of fluorescent tracers. Chem Eng J 264:389–398. https://doi.org/10.1016/j.cej.2014.11.073

Ning SZ (2013) Coal resources and tectonic division of ordos basin. In: Proc, 2nd International Conf on Energy and Environmental Protection (ICEEP 2013), Trans Tech Publications Ltd, Guilin, Peoples R China, pp 316-319

Pecly JOG (2018) Estimation of the dilution field near a marine outfall by using effluent turbidity as an environmental tracer and comparison with dye tracer data. Water Sci Technol 77:269–277. https://doi.org/10.2166/wst.2017.535

Peely AB, Mohammadi Z, Raeisi E (2021) Breakthrough curves of dye tracer tests in karst aquifers: review of effective parameters based on synthetic modeling and field data. J Hydrol 602:15. https://doi.org/10.1016/j.jhydrol.2021.126604

Pinasseau L, Mermillod-Blondin F, Fildier A, Fourel F, Vallier F, Guillard L, Wiest L, Volatier L (2023) Determination of groundwater origins and vulnerability based on multi-tracer investigations: new contributions from passive sampling and suspect screening approach. Sci Total Environ 876:12. https://doi.org/10.1016/j.scitotenv.2023.162750

Qamar A, Ul Haq I, Alhaisoni M, Qadri NN (2019) Detecting grounding grid orientation: transient electromagnetic approach. Appl Sci-Basel 9:15. https://doi.org/10.3390/app9245270

Qi JH, Xu M, Cen XY, Wang L, Zhang Q (2018) Characterization of karst conduit network using long-distance tracer test in Lijiang, southwestern China. Water 10:19. https://doi.org/10.3390/w10070949

Qiu HY, Hu R, Huang Y, Gwenzi W (2022) Detection and quantification of dam leakages based on tracer tests: a field case study. Water 14:17. https://doi.org/10.3390/w14091448

Qu S, Shi ZM, Liang XY, Wang GC, Jin XM (2021a) Origin and controlling factors of groundwater chemistry and quality in the Zhiluo aquifer system of northern Ordos Basin. China Environ Earth Sci 80:15. https://doi.org/10.1007/s12665-021-09735-y

Qu S, Shi ZM, Wang GC, Han JQ (2021b) Application of multiple approaches to investigate hydraulic connection in multiple aquifers system in coalfield. J Hydrol 595:13. https://doi.org/10.1016/j.jhydrol.2020.125673

Schiperski F, Zirlewagen J, Stange C, Tiehm A, Licha T, Scheytt T (2022) Transport-based source tracking of contaminants in a karst aquifer: model implementation, proof of concept, and application to event-based field data. Water Res 213:10. https://doi.org/10.1016/j.watres.2022.118145

Schubert M, Brueggemann L, Knoeller K, Schirmer M (2011) Using radon as an environmental tracer for estimating groundwater flow velocities in single-well tests. Water Resour Res 47:8. https://doi.org/10.1029/2010wr009572

Sommer W, Valstar J, van Gaans P, Grotenhuis T, Rijnaarts H (2013) The impact of aquifer heterogeneity on the performance of aquifer thermal energy storage. Water Resour Res 49:8128–8138. https://doi.org/10.1002/2013wr013677

State Bureau of Coal Industry (2000) Measuring method on height of water flowing fractured zone using loses of drilling fluid, MT/T865–2000. State Bureau of Coal Industry, Beijing (**in Chinese**)

Wang DJ, Qian JZ, Ma L, Xu HM, Wang XY, Wang YY (2022) Integration of multiple hydrogeological survey technologies for exploring the groundwater distribution in karst areas: a case study in Xingfu Spring, Chaohu city. China J Hydrol 614:11. https://doi.org/10.1016/j.jhydrol.2022.128637

Wolkersdorfer C, Göbel J, Hasche-Berger A (2016) Assessing subsurface flow hydraulics of a coal mine water bioremediation system using a multi-tracer approach. Int J Coal Geol 164:58–68. https://doi.org/10.1016/j.coal.2016.03.010

Yeh HF, Lin HI, Wu CS, Hsu KC, Lee JW, Lee CH (2015) Electrical resistivity tomography applied to groundwater aquifer at downstream of Chih-Ben Creek basin. Taiwan Environ Earth Sci 73:4681–4687. https://doi.org/10.1007/s12665-014-3752-1

Zeng YF, Meng SH, Wu Q, Mei AS, Bu WY (2023) Ecological water security impact of large coal base development and its protection. J Hydrol 619:18. https://doi.org/10.1016/j.jhydrol.2023.129319

Zeng YF, Mei A, Wu Q, Meng S, Zhao D, Hua Z (2024) Double verification and quantitative traceability: a solution for mixed mine water sources. J Hydrol 630:130725. https://doi.org/10.1016/j.jhydrol.2024.130725

Zhu J, Wang RH, Lin B (2010) Research on the phenomenon of multiple fracturing and fracture apertures of surrounding rock mass in deep roadway. J China Coal Soc 35(06):887–890. https://doi.org/10.13225/j.cnki.jccs.2010.06.005(inChinese)

Springer Nature or its licensor (e.g. a society or other partner) holds exclusive rights to this article under a publishing agreement with the author(s) or other rightsholder(s); author self-archiving of the accepted manuscript version of this article is solely governed by the terms of such publishing agreement and applicable law.